Epidermal Growth Factor from the Mouse. Structural Characterization by Proton Nuclear Magnetic Resonance and Nuclear Overhauser Experiments at 500 MHz†

K. H. Mayo*

ABSTRACT: Mouse epidermal growth factor (mEGF), a protein hormone effector molecule that regulates cellular development and division, has been investigated by using proton nuclear magnetic resonance techniques at 500 MHz. Well-resolved downfield aromatic and α-CH proton resonances (5.0–8.0 ppm) and an upfield ring current shifted isoleucine δ-methyl resonance ($\sim$0.5 ppm) have been examined by using principally nuclear Overhauser methods. The data are analyzed in terms of model building based on the predictive Chou–Fasman secondary structure algorithm applied to mEGF [Holladay, L. A., Savage, C. R., Cohen, S., & Puett, D. (1976) *Biochemistry 15*, 2624–2633], which suggests the existence of some β-structure and little or no α-helicity. Proximity relationships derived from nuclear Overhauser data among Tyr-3, -10, and -13, His-22, and Ile-23 allow refinement of some aspects of the predicted secondary structure and render additional information on how the protein backbone in mEGF is folded (i.e., tertiary structure). Nuclear Overhauser effects (NOEs) from irradiation of several α-CH proton resonances give evidence for tiered β-sheet structure in mEGF. Such proximity relationships derived from NOE data place stringent limitations on possible models for the molecule. pH titration data demonstrate a His-22 pK_a of 7.1, indicating either a salt bridge or hydrogen-bond formation between His-22 and another residue. The His-22 pK_a is also reflected in the chemical shift changes of several other resonances as a function of pH. Nuclear Overhauser methods, used to differentiate direct (protonation) and indirect (conformation) effects on the chemical shift changes in the spectra of mEGF by varying the pH, yield evidence for a pH-induced conformational transition in the protein hormone associated with the breaking of the His-22 salt bridge or hydrogen bond.

The observation in 1962 that newborn mice opened their eyes earlier than normal when injected with a crude preparation of homogenized mouse salivary glands led to the postulation of the existence of a growth-stimulating hormone. From this glandular extract was isolated the material responsible for the effect—the protein hormone now called mouse epidermal growth factor (mEGF)[1] (Cohen, 1962).

On a cellular level, mEGF works directly on skin cells by binding to a transmembrane receptor molecule and becoming internalized in the cell by endocytosis (Cohen et al., 1979; Carpenter & Cohen, 1976). Binding of mEGF to the receptor molecule in the presence of ATP also generates an enhanced phosphorylation of a number of membrane proteins; the formation of this mEGF–receptor complex (Hollenberg & Cutrecasas, 1973; Carpenter et al., 1975) most likely activates a protein kinase which is one part of the mEGF–receptor polypeptide chain (Buhrow et al., 1982, 1983). Physiological effects of mEGF include increased uptake of salts and glucose; increased protein, RNA, and DNA synthesis; and cell division. For a recent review, see Carpenter & Cohen (1979).

On a molecular level, mouse epidermal growth factor (mEGF) consists of a single polypeptide chain of 53 amino acid residues (6045 daltons) and contains three disulfide bonds (Taylor et al., 1972). The primary sequence of mEGF has been elucidated by Savage et al. (1973) and is devoid of lysine, alanine, and phenylalanine. Although the primary sequence of mEGF has been known for some time (Savage et al., 1973), efforts to crystallize it have failed; therefore, no X-ray crystal structure exists. mEGF has been characterized in a number of physicochemical studies (Taylor et al., 1970, 1972, 1974a,b). Holladay et al. (1976) have investigated the structural properties of mEGF by using circular dichroism and indicate the existence of about 22% β-structure and no α-helicity. These authors (Holladay et al., 1976) have also applied the predictive algorithm of Chou & Fasman (1974a,b, 1978a,b) to mEGF. The following regions of ordered secondary structure are predicted: two sections of β-structure, residues 19–23 and residues 29–37; one section of α-helix, residues 46–53; and chain reversals (β-turns) beginning at residues 3, 6, 10, 15, 27, 37, and 40. The predicted α-helical segment also has a high $\langle P_\beta \rangle$ value, and thus, some type of β-structure may be available as a viable alternative to the favored α-segment.

Many studies of structure–function relationships of a variety of polypeptide hormones have indicated that the biological activity of these molecules is stringently dependent on a precise chemical and physical structure. The long-range objectives of these investigations are, first of all, to study the solution structure of mEGF and then to identify how the conformation of this potent mitogen may be related to its biological effects and, finally, to elucidate which specific domain(s) in the structure of the peptide hormone is (are) essential for interaction with its membrane receptor.

The fact that this versatile protein contains only 53 amino acid residues, including one histidine, two tryptophans, five tyrosines, and no phenylalanine residues, makes this polypeptide an excellent choice for study by ^{1}H nuclear magnetic resonance (NMR) techniques. In this present study, the objective is to test and refine the proposed secondary structure of mEGF and to investigate some aspects of how the molecule

† From the Department of Chemistry, Yale University, New Haven, Connecticut 06511. *Received November 7, 1983.* This work was supported by a grant from the National Institutes of Health (GM-32243) and benefited from NMR facilities made available through Grant CHE-7916210 from the National Science Foundation.

* Address correspondence to this author at the Department of Chemistry, Temple University, Philadelphia, PA 19122.

[1] Abbreviations: mEGF, mouse epidermal growth factor; DSS, sodium 4,4-dimethyl-4-silapentanesulfonate; NOE, nuclear Overhauser effect; FID, free induction decay; rf, radio frequency.

0006-2960/84/0423-3960$01.50/0

is folded (i.e., tertiary structure). High-resolution ^1H NMR (500 MHz) methods, analogous to those applied to other small soluble proteins over the past few years (Gordon & Wüthrich, 1978; Poulsen et al., 1980; Wagner & Wüthrich, 1979; Dobons et al., 1980; Mayo et al., 1983), have been employed. Here, results based largely on nuclear Overhauser experiments (NOEs) (Noggle & Shirmer, 1971) on epidermal growth factor from mouse salivary glands (mEGF) are presented. Nuclear Overhauser effects contain much information about structural and dynamical properties of proteins (Sykes et al., 1974; Oldfield et al., 1975; Chapman et al., 1978; Krishna et al., 1978; Gordon & Wüthrich, 1978; Poulsen et al., 1980; Trapp, 1980). Dobson et al. (1980) and Poulsen et al. (1980) have recently shown that relative nuclear Overhauser effects measured after short periods of saturation of assigned resonances in the proton NMR spectrum of lysozyme at high field (498 MHz) can be directly correlated with the inverse sixth powers of interproton distances taken from the crystal structure. Under suitable conditions, therefore, NOEs can be interpreted in terms of interresidue proximity relationships with an aproximate range of 2.5–4.0 Å. The general characteristics of the predictive model of Chou and Fasman (Holladay et al., 1976) for mEGF can, therefore, be tested. In addition to a test of secondary structure, such NOE data can place stringent limitations on tertiary folding.

This present study also investigates the effect of pH on the NMR spectral properties of mEGF. Nuclear Overhauser experiments (NOEs) provide evidence for a pH-induced conformational (structural) transition in the protein and allow estimation of the extent of structural changes in the vicinity of several amino acid residues in mEGF. A possible biological significance of this structural transition in mEGF is also discussed.

Materials and Methods

Epidermal growth factor (EGF), purified from mouse salivary gland extracts by using the method of Savage & Cohen (1972), was generously provided by Professor Stanley Cohen, Vanderbilt University. Purity was checked by amino acid analysis, gel electrophoresis, and proton NMR.

Samples for ^1H NMR measurements were dissolved in D_2O to exchange all labile protons, lyophilized, and redissolved in D_2O immediately before the experiment. The final protein concentration was about 0.6 mM in approximately 10 mM potassium phosphate buffer. The pD was adjusted by adding microliter increments of NaOD or D_3PO_4 to a 0.5-mL sample. All measurements were done at pD values read directly from the pH meter and not adjusted for isotope effects (Kalinichenko, 1976; Bundi & Wüthrich, 1979). pH titration data were generated by random selection of a pD value to avoid the presence of systematic errors.

^1H NMR spectra were recorded in the Fourier mode on a Bruker WM-500 spectrometer at 303 K. The solvent deuterium signal was used as the field-frequency lock. NOEs were generated by irradiating the desired peak for times of 0.2, 0.4, 0.6, or 0.8 s at a power level sufficient to null z magnetization of the irradiated peak in 0.05 s. A 2-ms delay was introduced before accumulation to reduce transient effects, and a time of 3.5 s was allowed between the beginnings of accumulations to allow for recovery of z magnetization. Difference spectra were obtained by subtracting the free induction decay (FID) of the irradiated peak spectrum from the FID of a control spectrum which had been irradiated in a region where no resonances occur under the same experimental conditions. NOEs were determined by dividing areas of peaks in the difference spectrum by the area of the irradiated peak and correcting for differences in the numbers of protons.

Results

Spectral Assignments and the Effect of pH. The 500-MHz ^1H NMR spectrum of mouse epidermal growth factor (mEGF) in 10 mM potassium phosphate at pH 8.6 and 303 K (after exchange of all labile protons by D_2O) is shown in Figure 1a. This typical protein NMR spectrum shows many overlapping resonance lines between approximately 0.5 and 5.5 ppm and a better resolved aromatic region between 5.5 and 8.5 ppm. Lowering the pH to 5.7 (Figure 1b) modified the overall spectral characteristics of mEGF very little. All chemical shifts are given in parts per million (ppm) downfield from sodium 4,4-dimethyl-4-silapentanesulfonate (DSS).

Since most resonances upfield of the HDO resonance suffer from extensive overlap, they are indistinguishable and unassignable. At pH 8.6, two exceptions can be found. One of these is a far upfield, most likely ring current shifted, triplet resonance of intensity 3 found at 0.48 ppm (M) (Figure 1a). The only amino acid residue possessing a group of three protons spin coupled to two other protons giving a triplet resonance of intensity 3 is that of a δ-methyl group belonging to an isoleucine residue. Only two isoleucine residues are present in mEGF, Ile-23 and -35. Resonance M is, therefore, assignable to the δ-methyl group of either one of these two isoleucines.

The second tentatively assignable upfield resonance is resonance L (1.78 ppm) (Figure 1a). Due to the character of this resonance being a sharp singlet and the fact that it lies in the chemical shift region where the ϵ-methyl proton resonance of methionine residues is found, resonance L is tentatively assigned to the ϵ-methyl group of the only methionine present in mEGF, Met-21.

The low-field resonances of the aromatic amino acids are clearly resolved (Figure 2), and they must account for the corresponding 32 protons of the rings of the eight aromatic amino acids present in mEGF: histidine-22, tryptophan-49 and -50, and tyrosine-3, -10, -13, -29, and -37. The resonances can be assigned as follows: At pH 8.6, the single proton resonance at 7.4 ppm (A1) must be due to the C(2) proton of histidine-22 since it shifts approximately 1 ppm to lower field as the pH is lowered (Figure 2). Histidine is the only amino acid with a pK_a in this region. At pH 7.6, the less deshielded C(4) proton (A2) of histidine-22 can be seen at 5.84 ppm. This peak also shifts to lower field if the pH is lowered and is a one-proton resonance (Figure 2).

Resonances B1 and C1 at 7.27 and 7.22 ppm, respectively, are clearly doublets of intensity 1, each having coupling constants, J, of approximately 7 Hz. Of the aromatic protons, only the C(4) or C(7) protons of tryptophan residues are expected to be doublets of intensity 1 occurring this far downfield. Spin decoupling experiments show the tryptophan doublet resonance at 7.22 ppm (C1) to be scalar coupled to a triplet resonance of intensity 1 at 7.06 ppm (C2) which is in turn coupled to another triplet resonance of intensity 1 at 6.93 ppm (C3); this final triplet is lastly coupled to another doublet resonance of intensity 1 at 6.84 ppm (C4). Resonance C1 is thus assigned to the C(4) proton of a tryptophan residue since its chemical shift matches those cited in the literature for a Trp C(4) proton resonance; the other resonances follow suit: C2, C3, and C4 to the C(5), C(6), and C(7) protons, respectively, of one of the two tryptophan residues. The residue giving rise to these resonances will be called Trp-II.

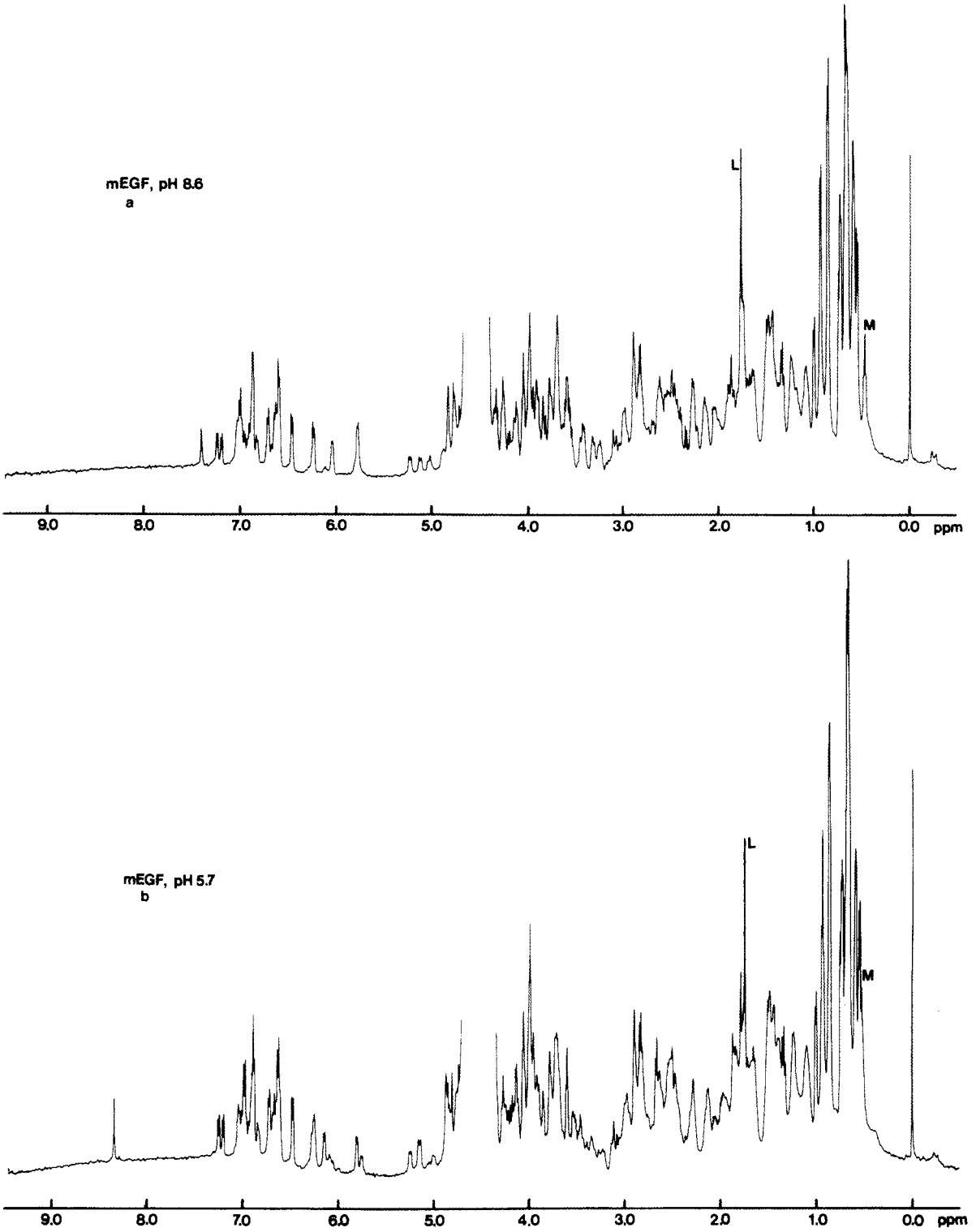

FIGURE 1: NMR spectra at 500 MHz of mEGF. The spectra represent 512 accumulations over a period of approximately 12 min using a 90° pulse on a 0.5-mL sample at concentrations of 0.6 mM mEGF in 10 mM KH_2PO_4, pH 8.6 (a) and pH 5.7 (b) at 303 K. The large, central HDO resonance has been omitted for clarity.

Resonance B1 is then, by the same reasoning as above, assigned to the C(4) proton of the only other tryptophan residue present in mEGF (Trp-I). Spin decoupling experiments again show this single proton doublet resonance (B1) to be coupled to a single proton triplet resonance at 7.04 ppm (B2), and, in turn, it is scaler spin coupled to another triplet resonance of intensity 1 at 6.90 ppm (B3), and, for the completion of this cycle, the B3 triplet resonance is shown to be coupled to a single proton doublet at 6.69 ppm (B4). The assignments follow as was the case for the Trp-II proton resonances: B2, B3, and B4 to the C(5), C(6), and C(7) protons, respectively, of Trp-I.

Both Trp-I and Trp-II have C(2)H single proton resonances which are spin coupled to no other protons and, therefore, are present in an NMR spectrum as singlets. Spin decoupling experiments cannot be used in this case; one must, therefore, rely on other methods like nuclear Overhauser experiments to provide this information. Two singlet resonances, other than those belonging to the His-22 C(2) and C(4) protons, are present in the spectrum at 6.82 and 6.91 ppm and are, by deduction, assignable to the two C(2)H proton resonances of Trp-I and Trp-II. At this time, the assignment of these res-

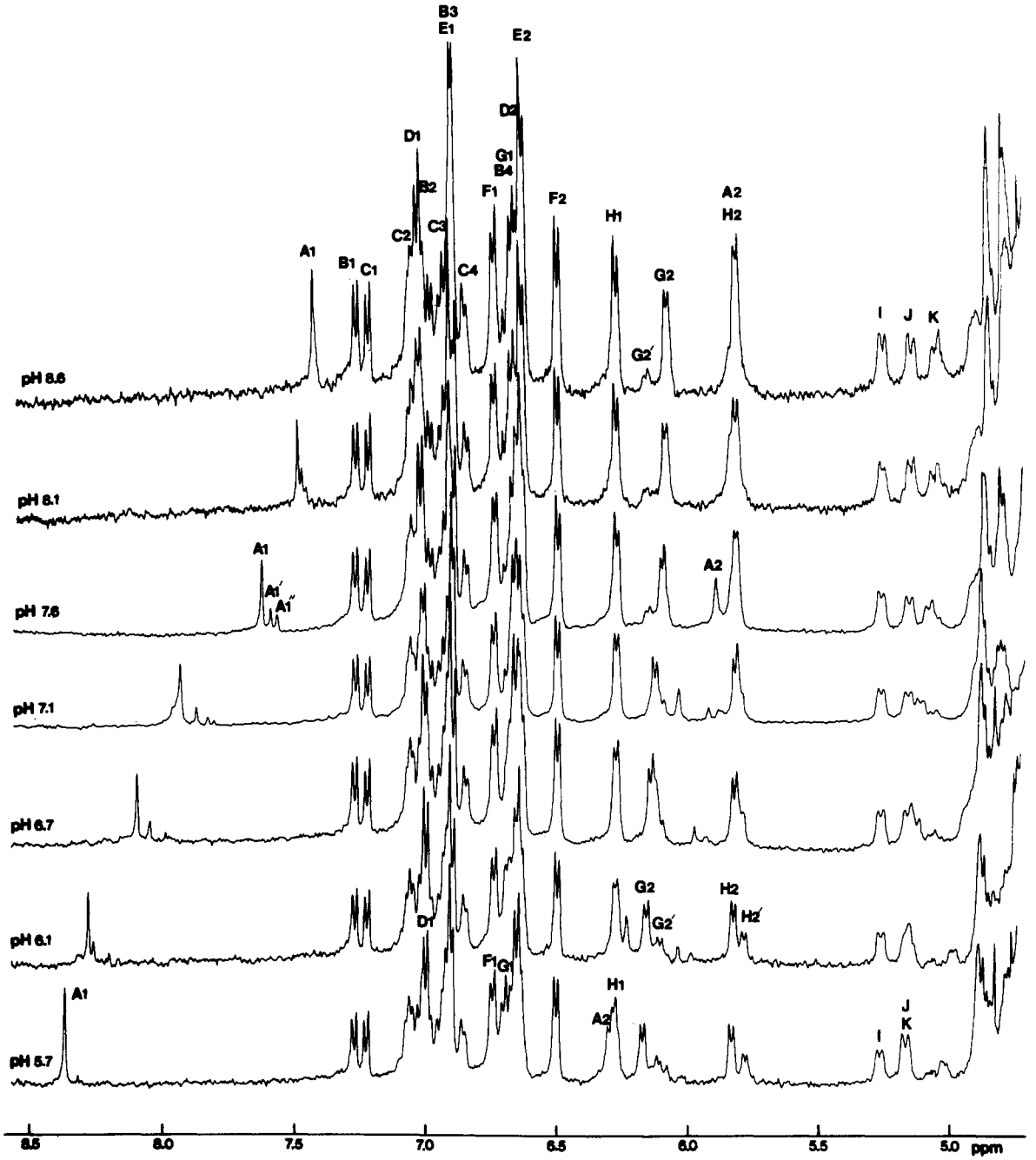

FIGURE 2: pH dependence of the downfield aromatic and partial α-CH proton regions. Spectra are presented showing chemical shift changes as the pH is varied. The pH of each individual spectrum is as indicated in the figure. Conditions are otherwise identical with those in Figure 1.

onances to either tryptophan-49 or tryptophan-50 is impossible. Both tryptophans are, however, present as neighbors at the C-terminal end of the primary sequence of mEGF (i.e., Trp-49 and -50) and provide nuclear probes of this region in mEGF.

The final aromatic resonances to be assigned are those arising from the five tyrosine residues present in mEGF (i.e., tyrosine-3, -10, -13, -29, and -37). Of the remaining resonances in the aromatic region of the spectrum (Figure 2), all of the resolved resonances are doublets of intensity 2, each showing a splitting of about 7 Hz. These spectral characteristics are typical for the 2,6 and 3,5 protons of tyrosine rings showing an AA'BB'-type spectrum. Such a spectrum can result from fast flipping on the NMR time scale of the aromatic ring around the C_β–C_γ bond (Wagner & Wüthrich, 1975). Spin decoupling experiments have grouped the tyrosine resonances in the following way, with the 2,6 proton resonance being assumed the most deshielded relative to the 3,5 proton resonance: D1 and D2 at 7.02 and 6.65 ppm to the 2,6 and 3,5 protons, respectively, of Tyr-I; E1 and E2 at 6.90 and 6.63 ppm to the 2,6 and 3,5 protons, respectively, of Tyr-II; F1 and F2 at 6.74 and 6.49 ppm to the 2,6 and 3,5 protons, respectively, of Tyr-III; G1 and G2 at 6.67 and 6.09 ppm to the 2,6 and 3,5 protons, respectively, of Tyr-IV; H1 and H2 at 6.27 and 5.81 ppm to the 2,6 and 3,5 protons, respectively, of Tyr-V.

Three single proton resonances slightly downfield of the HDO resonance (i.e., I, J, and K) are also readily assignable to α-CH protons belonging either to aromatic residues or to residues conformed in some type of β-structure.

These assignments have been summarized in Table I. Tentative assignments to specific amino acid residues given in Table I will be justified in the following text.

As is readily apparent in Figures 1 and 2, several resonances have been shifted by changes in pH. The more complete pH titration profile of the downfield aromatic proton region and

Table I: Resonance Assignments and NOE Connectivities at pH 7.9

peak	assignment	chemical shift (ppm)	NOE obsd on resonance[a]
	Aromatic Region		
A1	His-22 C(2)	7.56	M1
A2	His-22 C(4)	5.86	E2, M3
B1	Trp-I C(4)	7.27	
B2	Trp-I C(5)	7.00	
B3	Trp-I C(6)	6.90	
B4	Trp-I C(7)	6.69	
C1	Trp-II C(4)	7.22	
C2	Trp-II C(5)	7.06	
C3	Trp-II C(6)	6.93	
C4	Trp-II C(7)	6.84	
D1	Tyr-I 2,6	7.02	
D2	Tyr-I 3,5	6.65	
E1	Tyr-3 (or Tyr-II) 2,6	6.90	H1, H2, M1, M3
E2	Tyr-3 (or Tyr-II) 3,5	6.63	
F1	Tyr-III 2,6	6.74	
F2	Tyr-III 3,5	6.49	
G1	Tyr-13 (or Tyr-IV) 2,6	6.67	
G2	Tyr-13 (or Tyr-IV) 3,5	6.09	H2
H1	Tyr-10 (or Tyr-V) 2,6	6.27	E1, E2, H1a
H2	Tyr-10 (or Tyr-V) 3,5	5.81	E1, E2
	α-CH, β-CH_2, and Other Aliphatic Protons		
I	α-CH (tiered β-sheet)	5.26	F1, F2
I1	α-CH (tiered β-sheet)	4.03	
I2	β- or γ-CH	2.81	
J	α-CH (tiered β-sheet)	5.15	
J1	α-CH (tiered β-sheet)	4.90	
J2	β- or γ-CH	2.65	
J3	β- or γ-CH	2.46	
K	α-CH (tiered β-sheet)	5.06	G1, G2, H2
K1	β- or γ-CH	2.27	
K2	β- or γ-CH	2.20	
H1a	α-CH or Ser β-CH_2 (?)	3.97	
L	Met-21 ϵ-CH_3	1.78	
M	Ile-23 (or Ile-I) δ-CH_3	0.48	E1, E2
M1 (A1a, E1a)	α-CH	3.86	
M2	β- or γ-CH	2.75	
M3 (A2b)	β- or γ-CH	2.64	

[a] Only those resonances concerning interresidue NOEs, key to the structural interpretation presented here, have been listed.

some α-CH proton resonances shown in Figure 2 demonstrates, for example, that resonances K (an α-CH proton resonance) and G2 (the Tyr-IV 3,5 proton resonance) have each been downfield chemically shifted on the order of 0.1 ppm by lowering the pH from 8.6 to 5.7.

Slight chemical shift changes in the spectra presented in Figure 2 as a function of pH also occur in other resonances. The difference spectrum shown in Figure 3 was accomplished by subtracting the NMR spectrum at pH 8.6 from the one at pH 5.7 to observe the full extent of chemical shift changes of resonances in this region as a result of varying the pH. The top part of the difference spectrum (Figure 3) represents resonances at pH 5.7 which display different chemical shiifts from resonances observed at pH 8.6 shown in the bottom part of the difference spectrum. Resonances are labeled as in Figure 2. Aside from those resonances whose pH-induced chemical shift changes have been previously discussed (i.e., resonances A1, A2, G2, and K), several other resonances are observed to also have been affected by pH changes.

Figure 4 presents plots of the chemical shift (in ppm) vs. pH for those resonances whose chemical shift changes observed in Figure 3 as a function of pH are significant. These include the His-22 C(2) (A1) and C(4) (A2) proton resonances as well as resonances D1 (Tyr-I 2,6 protons), E1 (Tyr-II 2,6 protons), G2 (Tyr-IV 3,5 protons), K (α-CH proton), L (Met-21 ϵ-CH_3 proton), and M (Ile-23 δ-CH_3 proton). The His-22 C(2) and C(4) titration plots demonstrate a pK_a value for the His-22 residue of approximately 7.1 (Figure 4a). For a histidine residue free in solution or not hydrogen bonded to any other residue, a pK_a of approximately 6.0 is normally achieved. This present pK_a of 7.1, more than 1 pH unit removed from that of the free histidine species, indicates that His-22 either is not solvent exposed or exists in some type of hydrogen-bond or salt bridge formation. The latter explanation is favored since a protein of this size (i.e., a polypeptide of 53 amino acid residues) would not be expected to have an extensive central, non-solvent-exposed region. It is felt, therefore, that a hydrogen bond or salt bridge between His-22 and some other residue exists below pH 7.1 and is titrated above pH 7.1. It is unclear whether or not the other residue which interacts with His-22 is a carboxylate anion (i.e., negatively charged). It is equally possible that simple hydrogen bonding of one of the imidazolium NH moieties to another residue exists. Throughout the rest of this paper, this salt bridge or hydrogen bond shall be referred to as the His-22 interresidue linkage.

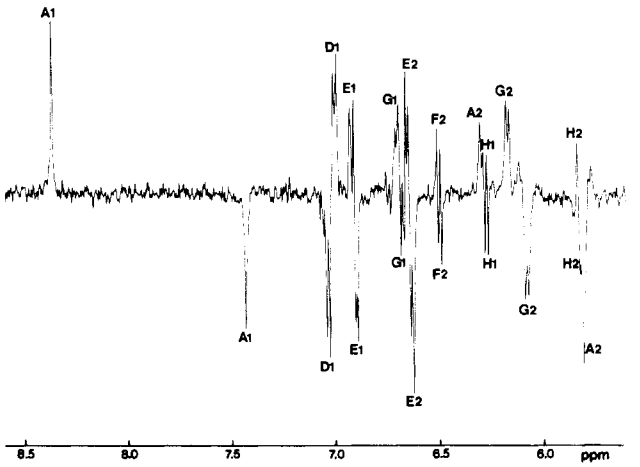

FIGURE 3: Difference spectrum of the downfield aromatic region generated by subtracting the NMR spectrum taken at pH 5.7 (top resonances) from the NMR spectrum taken at pH 8.6 (bottom resonances). Resonances are labeled as described in the text.

The His-22 pK_a of 7.1 is found, furthermore, to be reflected in the chemical shift changes of all resonances plotted in Figure 4 as a function of pH. From the standpoint of chemical shift changes in these resonances as a function of pH, either a direct (protonation) or an indirect (conformational) effect could account for this observation. Ile-23 and Met-21, for example, are located on one side or the other of His-22 in the primary sequence of mEGF; a change in the charge of His-22 from +1 to 0 on titration of the His-22 proton could possibly account for the chemical shift changes of resonances L (the Met-21 ϵ-CH_3 resonance) and M (the Ile-23 δ-CH_3 resonance) as a function of pH. These changes in the chemical shift as a function of pH could, then, be examples of a direct (protonation) effect. The pK_a of 7.1 reflected in the chemical shift changes as a function of pH for other resonances could be the result of either indirect or direct effects. Direct and indirect effects are, to say the very least, not easily differentiated. Structural changes between two or more conformations in question in a protein must be clearly demonstrated before an interpretation of an indirect (conformational) effect can usually be made.

Minor Spectral Resonances. The pH-induced appearance of several minor spectral resonances associated with their respective major spectral resonances cannot be readily explained (Figure 2). Their existence could be the result either

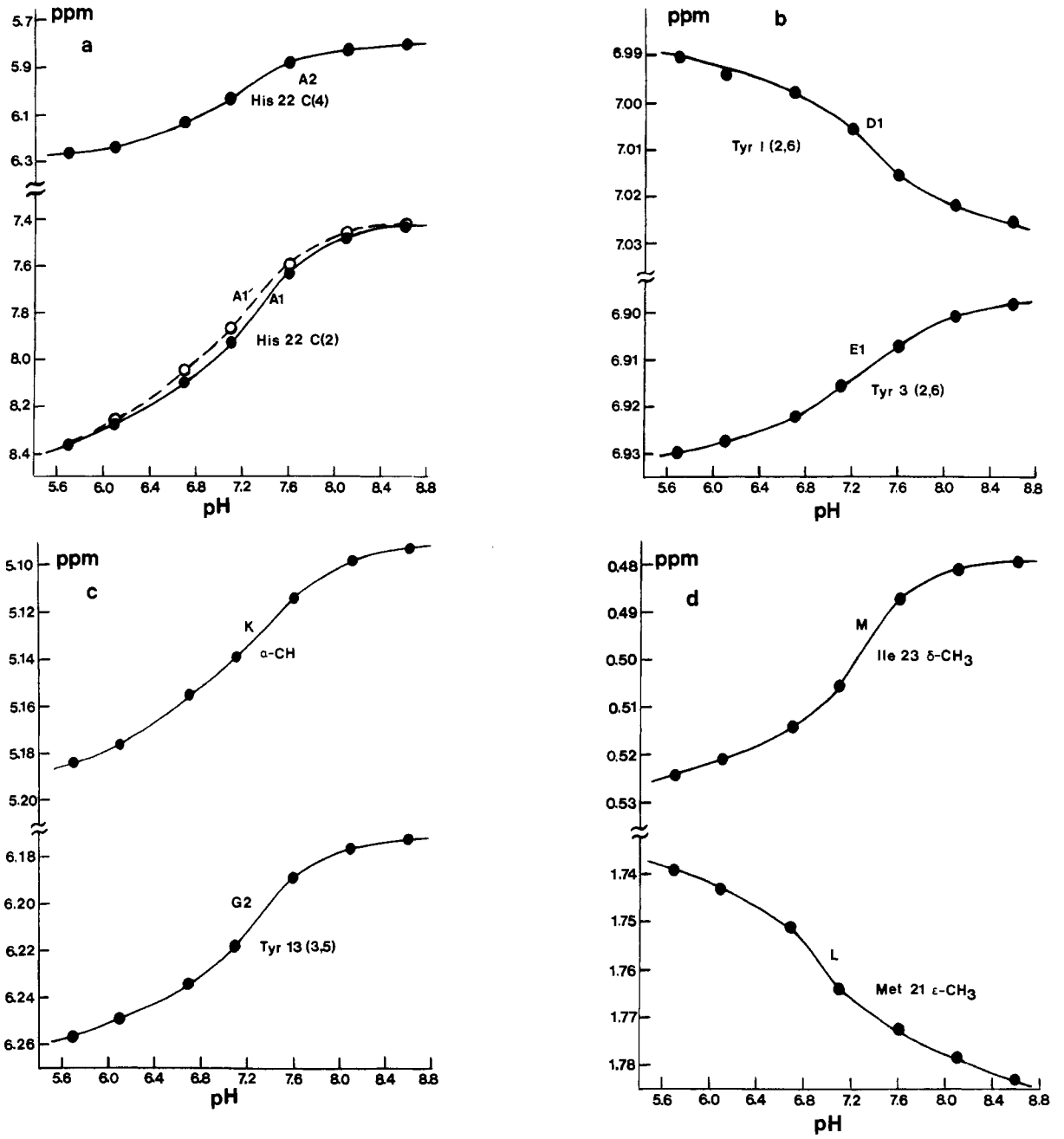

FIGURE 4: pH dependence of the chemical shifts. The chemical shift (in ppm) is plotted vs. pH for resonances A1 and A2 (a), D1 and E1 (b), G2 and K (c), and L and M (d). Closed and opened circles represent experimental points. Curves drawn through the circles have been drawn only as a visual aid.

of sequence heterogeneity (i.e., an amino acid substitution difference between various mEGF molecules) or of conformational heterogeneity.

At least two minor resonances (A1′ and A1″) can be clearly seen to be associated with the major His-22 C(2) proton resonance (A1) (Figure 2). Resonance A1′ represents approximately 10–15% of the total His-22 C(2) proton resonance population. The pK_a of this minor fraction is shifted slightly to a lower pH value of 6.9 (Figure 4a).

The Tyr-IV 3,5 proton resonance (G2) has, likewise, a minor resonance associated with it (G2′) which is upfield shifted as the pH is lowered, unlike its major resonance counterpart which is downfield chemically shifted as the pH is lowered. An estimate of the pK_a of the minor resonance (G2′) is impossible due to spectral overlap of the major (G2) and minor (G2′) resonances over the pH range investigated.

Another minor resonance resolved at low pH values is resonance H2′, associated with the major Tyr-V 3,5 proton resonance (H2). This minor resonance (H2′) shifts monotonically upfield as the pH is lowered.

Other pH-induced resolution of minor spectral resonances may well occur. Due to the extent of spectral overlap in the upfield region, observation of these minor resonances in this spectral region is hindered. Other well-resolved downfield resonances have no observable minor spectral resonances associated with them. The nature of this present study has been, in any event, undertaken on the major conformational population. Furthermore, since most resonances do not exhibit this minor heterogeneity, whatever structural alterations exist must be fairly localized.

Nuclear Overhauser Experiments. (A) Structural Analysis and Resonance Assignments. Since several downfield tyrosine proton resonances (i.e., the Tyr-III 3,5, Tyr-IV 3,5, and Tyr-V 2,6 and 3,5 protons, peaks F2, G2, H1, and H2, respectively) are well resolved, a logical starting point for structural analysis using selective NOE experiments is at hand. NOE difference

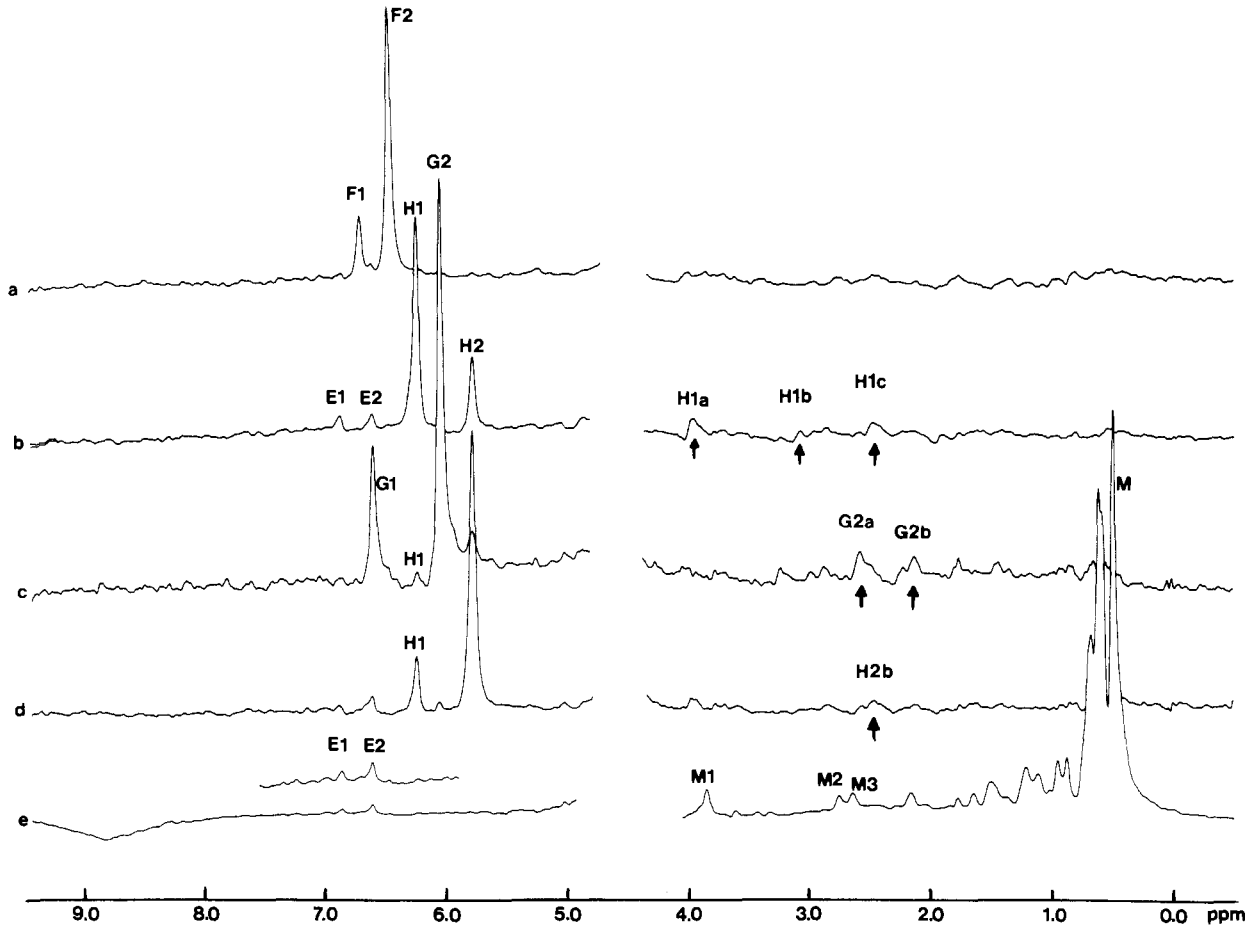

FIGURE 5: NOEs given by mEGF. Five NOE difference spectra are shown, each representing the difference between an accumulation of 1500 FIDs taken with saturating rf off-resonance and another accumulation of 1500 FIDs taken with saturating rf on-resonance. In each case, the rf saturation time was 0.6 s. Spectra are for saturation of resonances F2 (a), H1 (b), G2 (c), H2 (d), and M (e). Labeling of resonances is as in Figures 1 and 2 and as described in the text. Sample conditions are as described in Figure 1.

spectra at pH 7.9 and 303 K obtained by subtracting spectra with radio-frequencey (rf) irradiation on and off each of the four above-mentioned tyrosine proton resonances for 0.6 s are presented in Figure 5a–d.

Irradiation of the Tyr-III 3,5 proton resonance (F2) (Figure 5a) shows a strong NOE at the Tyr-III 2,6 proton resonance (F1). The NOE on the 2,6 proton resonance when the 3,5 proton resonance is irradiated and vice versa (i.e., an NOE on the 3,5 proton resonance when the 2,6 proton resonance is irradiated) is not unexpected since the 2–3 and 5–6 pairs are only 2.4. Å distant from one another. Several other minor NOEs are discernible on nonassigned resonances in the upfield part of the spectrum, although no readily interpretable information is gained from them.

Figure 5b, on the other hand, demonstrates that irradiation of the Tyr-V 2,6 proton resonance (H1) not only gives the expected NOE on its own 3,5 proton resonance (H2) but also shows NOEs on both the Tyr-II 2,6 and Tyr-II 3,5 proton resonances (i.e., peaks E1 and E2, respectively). A further NOE at resonance H1a at 3.97 ppm (i.e., the α-CH proton resonance region) most likely arises from an α-CH within a distance of 4 Å from the Tyr-V 2,6 protons but may, on the basis of chemical shift data, also arise from the β-CH_2 protons of a serine residue. The presence of NOEs among the Tyr-V 2,6 and Tyr-II 2,6 and 3,5 proton resonances suggests proximity of these residues. Furthermore, irradiation of the Tyr-V 3,5 proton resonance (H2) (Figure 5d) shows NOEs to the Tyr-II 2,6 and 3,5 proton resonances (i.e., peaks E1 and E2, respectively), providing further confirmation of the proximity relationship between Tyr-V and Tyr-II.

Irradiation of the Tyr-IV 3,5 proton resonance (G2) gives the expected NOE at the Tyr-IV 2,6 proton resonance (G1) (Figure 5c). Intensity changes are noted at positions on the Tyr-V 2,6 (H1) and 3,5 (H2) proton resonances. These resonances, however, are spectrally located so close to one another that the possibility of direct saturation from irradiation of the Tyr-IV 3,5 proton resonance remains. Two pieces of information indicate the NOE at the Tyr-V 3,5 proton resonance to be real. First of all, resonance G2 (i.e., Tyr-IV 3,5) is spectrally closer to resonance H1 (Tyr-V 2,6) than it is to resonance H2 (Tyr-V 3,5), and the difference spectrum (Figure 5c) indicates the intensity of resonance H2 to be almost a factor of 2 larger than the intensity of resonance H1. Second, control experiments were performed where irradiation between these two close, yet well-resolved, resonances was carried out. Intensity changes were approximately a factor of 3 less than that seen in Figure 5c. In other words, these data indicate that Tyr-IV and Tyr-V are ca. 3–4 Å apart and provide an additional piece of structural information, namely, that a second tyrosine residue (i.e., Tyr-IV) is conformed near Tyr-V.

Further desired structural information is gained through irradiation of the apparently upfield, ring current shifted Ile-I δ-CH_3 resonance (M) (Figure 5e). This experiment, which unfortunately results in partial saturation of resonances around 0.7 ppm in addition to resonance M, gives NOEs at the Tyr-II 2,6 and 3,5 proton resonances (i.e., peaks E1 and E2, respectively) as well as at several other upfield resonances around 1 ppm. One strong NOE (resonance M1) is observed in the α-CH region at 3.86 ppm.

Only two isoleucine residues are present in mEGF (i.e.,

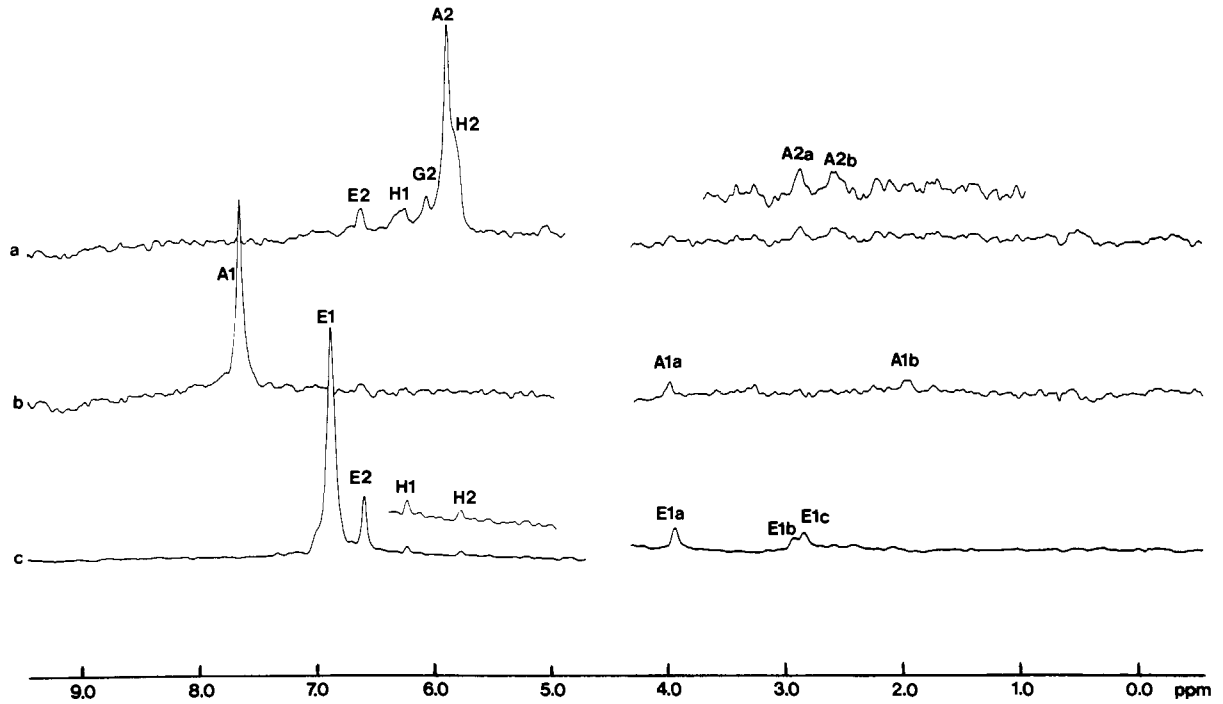

FIGURE 6: NOEs given by mEGF. Three NOE difference spectra are shown with accumulations as described in Figure 3. Spectra are for saturation of resonance A2 (a), resonance A1 (b), and resonance E1 (c). Sample conditions are as described in Figure 1, except at pH 7.4.

Ile-23 and -35). The existence of NOEs at resonances arising from the Tyr-II 2,6 and 3,5 protons when the Ile-I δ-CH_3 proton resonance is irradiated places strict limitations on the possible allowed conformations (tertiary structure) of mEGF.

Additional structural information is gained from irradiation of the His-22 C(4) (A2) and C(2) (A1) proton resonances (i.e., spectra a and b, respectively, of Figure 6). For these experiments, the pH was slightly lowered to pH 7.4 in order to resolve the His-22 C(4) proton resonance (A2) from the Tyr-V 3,5 proton resonance (H2), while still remaining above the His-22 pK_a of approximately 7.1. Irradiation of resonance A2 [i.e., the His-22 C(4) proton resonance] (Figure 6a) produces several NOEs of which two can be dismissed (i.e., H1 and G2) due to direct saturation of resonance H2 and themselves. The large NOE on resonance E2 (i.e., the Tyr-II 3,5 proton resonance) is quite real, on the basis of both off-resonance control experiments and the absence of any apparent amplitude for resonance F2 in the difference spectrum (Figure 6a). This piece of structural information clearly indicates a proximity relationship between Tyr-II and His-22. Two other NOEs appear upfield of the HDO resonance (i.e., resonances A2a and A2b). Resonance A2b has the same chemical shift as resonance M3 observed on irradiation of the upfield Ile-I δ-methyl triplet resonance (Figure 5e). Since a proximity relationship has already been established between Tyr-II and the Ile-I δ-methyl group, it is very likely that resonances A2b and M3 are identical.

Irradiation of the His-22 C(2) resonance (A1) (Figure 6b) gives NOEs at two upfield resonances (i.e., A1a and A1b). Resonance A1a exhibits the same chemical shift as resonance M1 from the Ile-I δ-methyl triplet resonance irradiation (Figure 5e). Again, reasoned by proximity relationships among Tyr-II, Ile-I, and His-22, resonances A1a and M1 are probably identical.

Although irradiation of overlapping resonances has been avoided in this study, irradiation of resonance E1 (i.e., the Tyr-II 2,6 proton resonance) was performed (Figure 6c) for confirmatory evidence of previously observed NOEs. This experiment (i.e., irradiation of resonance E1; Figure 6c) gave NOEs at the Tyr-V 2,6 and 3,5 proton resonances (i.e., H1 and H2, respectively) as well as at three upfield resonances (i.e., E1a, E1b, and E1c). Resonances E1a and E1b exhibit the same chemical shifts as resonances A1a (M1) and A2a, respectively, and are likely identical with these resonances. These NOEs confirm the above-discussed structural results in regard to proximity relationships among Tyr-II, Tyr-V, Ile-I, and His-22. Upon irradiation of the isoleucine-I δ-CH_3 resonance M, NOEs were observed at the Tyr-II 2,6 and 3,5 proton resonances (i.e., E1 and E2, respectively) (Figure 5e). The absence of any discernible NOE at resonance M (i.e., Ile-I δ-CH_3) upon irradiation of resonance E1 (i.e., the Tyr-II 2,6 proton resonance) (Figure 6c) is likely the result of an efficient internal relaxation mechanism for the methyl group.

Irradiation of resonances B1 and C1 [i.e., the Trp-I and -II (C(4) proton resonances, respectively], while well resolved in themselves, produces only NOEs at their own neighboring tryptophan ring resonances and provides no structural information. These data have not been presented for this reason.

Three well-resolved α-CH proton resonances (i.e., I, J, and K at 5.26, 5.15, and 5.06 ppm, respectively) appear in the NMR spectra of mEGF (Figures 1 and 2). At pH 8.6, two of these three resonances appear to be doublets of intensity 1 (i.e., I and J), while the third one, resonance K, appears to be a triplet of intensity 1 (Figure 2). The fact that their chemical shifts are strongly downfield shifted from the majority of α-CH proton resonances may be the result of their being either aromatic α-CH protons or α-CH protons conformed in some type of β-structure, or a combination of the two aforementioned possibilities. The apparent doublets could indicate the α-CH proton to be spin coupled to only one other proton (i.e., a β-CH proton in this case). It is also possible that this is an unresolved doublet of doublets produced by a particular preferred conformation of a β-CH_2 group giving couplings of 2 and 10 Hz. The only amino acid residues whose α-CH protons are spin coupled to only one other proton (i.e., a β-CH proton) are isoleucine, valine, and threonine. The coupling constants ($J_{\alpha CH\beta}$) of these resonances are in the range of 8–10 Hz and, using the Karplus relationships, indicate a dihedral

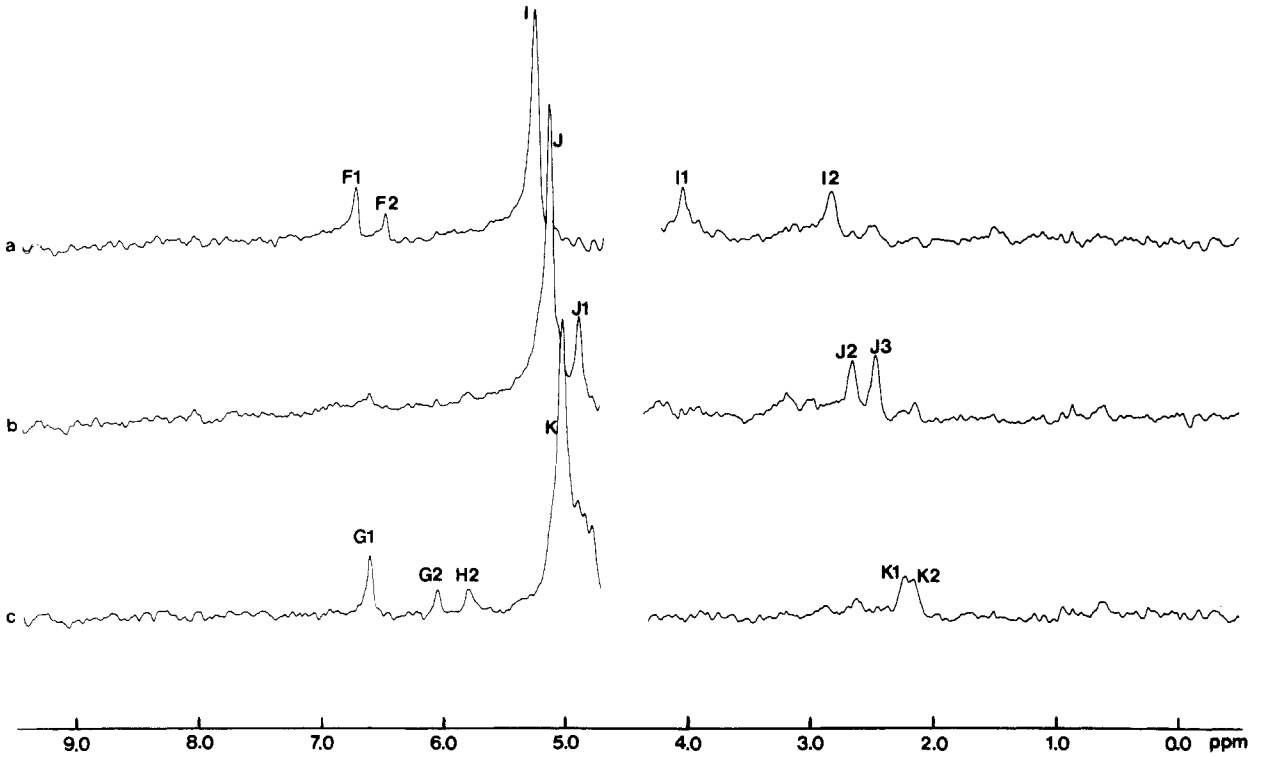

FIGURE 7: NOEs given by mEGF. Three NOE difference spectra are shown with accumulations as described in Figure 3. Spectra are for saturation of resonance I (a), resonance J (b), and resonance K (c). Sample conditions are as described in Figure 1.

angle between the α-CH and β-CH protons of nearly 180°.

Irradiation of resonance I (Figure 7a) produces NOEs at the Tyr-III 2,6 and 3,5 proton resonances (i.e., resonances F1 and F2, respectively), as well as at two further upfield resonances, I1 and I2. Resonance I1 at 4.07 ppm seems clearly assignable to an α-CH proton, and resonance I2 at 2.81 ppm probably belongs to a β-CH proton. The presence of an NOE of this magnitude between two α-CH proton resonances (i.e., I and I1) is indicative of the α-CH protons associated with these resonances being conformed in a β-sheet structure (Wüthrich et al., 1982; Billeter et al., 1982). Further structural information is derived from NOEs on the Tyr-III 2,6 and 3,5 proton resonances. Whether or not resonance I is the Tyr-III α-CH proton resonance, proximity would make it probable that Tyr-III would also be involved in this β-sheet region. The NOE on the Tyr-III 3,5 proton resonance when the α-CH proton resonance I is irradiated reduces the probability that resonance I is our Tyr-III α-CH proton resonance. The normal time development of these NOE data makes spin diffusion unlikely, and it is unlikely that a strong NOE could exist between these more remote ring protons and the residue's own α-CH proton.

Resonance J was next irradiated (Figure 7b). The α-CH proton associated with this resonance is also conformed in a β-sheet structure by virtue of the fact that a clear strong NOE is observed to the α-CH proton resonance J1 (Wüthrich et al., 1982; Billeter et al., 1982). Large NOEs at two other upfield resonances (i.e., J2 and J3) were also observed. These resonances probably belong to β- or γ-CH protons.

Finally, irradiation of the α-CH proton resonance K (Figure 7c) produces several NOEs and more structural information. NOEs are observed on the Tyr-IV 2,6 (G1) and 3,5 (G2) proton resonances, as well as on the Tyr-V 3,5 (H2) proton resonance and on two upfield resonances (i.e., K1 and K2). The NOEs at all three of these tyrosine resonances (i.e., Tyr-IV 2,6 and 3,5 and Tyr-V 3,5) follow a normal NOE time development curve (results not shown) (Poulsen et al., 1979; Mayo et al., 1983) and are not the result of spin diffusion. As presented above, a proximity relationship between Tyr-IV and Tyr-V was already demonstrated, and this piece of data now stands as confirmatory evidence. If one places both tyrosine residues in an antiparallel β-sheet structure, the three NOEs at these two tyrosine residues can be accounted for by proximity relationships with a neighboring α-CH proton. Resonances K1 and K2 belong most likely to either β- or γ-CH protons. Key interresidue NOE proximity relationships have been summarized in Table I.

(B) Direct and Indirect Effects of pH. In order to possibly differentiate between indirect (conformational) and direct (protonation) effects on the NMR spectral properties of mEGF induced by varying the pH, nuclear Overhauser experiments on well-resolved tyrosine resonances were performed (i.e., resonances F2, H1, G2, and H2) at a lower pH value of 6.0. Since nuclear Overhauser effects (NOEs) contain information about structural properties of proteins (Sykes et al., 1974; Oldfield et al., 1975; Chapman et al., 1978; Krishna et al., 1974; Gordon & Wüthrich, 1978; Poulsen et al., 1980: Dobson et al., 1980), a comparison of NOE data taken under varying environmental conditions (i.e., in this case pH changes) can provide strong evidence for the presence or absence of structural changes. NOE difference spectra acquired at 303 K and pH 6.0 obtained by subtracting spectra with rf irradiation on and off a resonance of interest for 0.4 s are presented in Figure 8a–d. These NOE data should be compared to those in Figure 5a–d taken at pH 7.9.

Irradiation of the Tyr-III 3,5 proton resonance (F2) at pH 6.0 (Figure 8a) shows a large NOE at its own 2,6 proton resonance (F1). Comparison of Figure 8a with Figure 5a which also shows irradiation of the Tyr-III 3,5 proton resonance (F2), but at pH 7.9, demonstrates similar NOE results at this higher pH value. The NOE on resonance F1 (i.e., the Tyr-III 2,6 proton resonance), as expected, remains unchanged. Other discernible minor NOEs in the difference spectra upfield of the HDO resonance are present, although differences be-

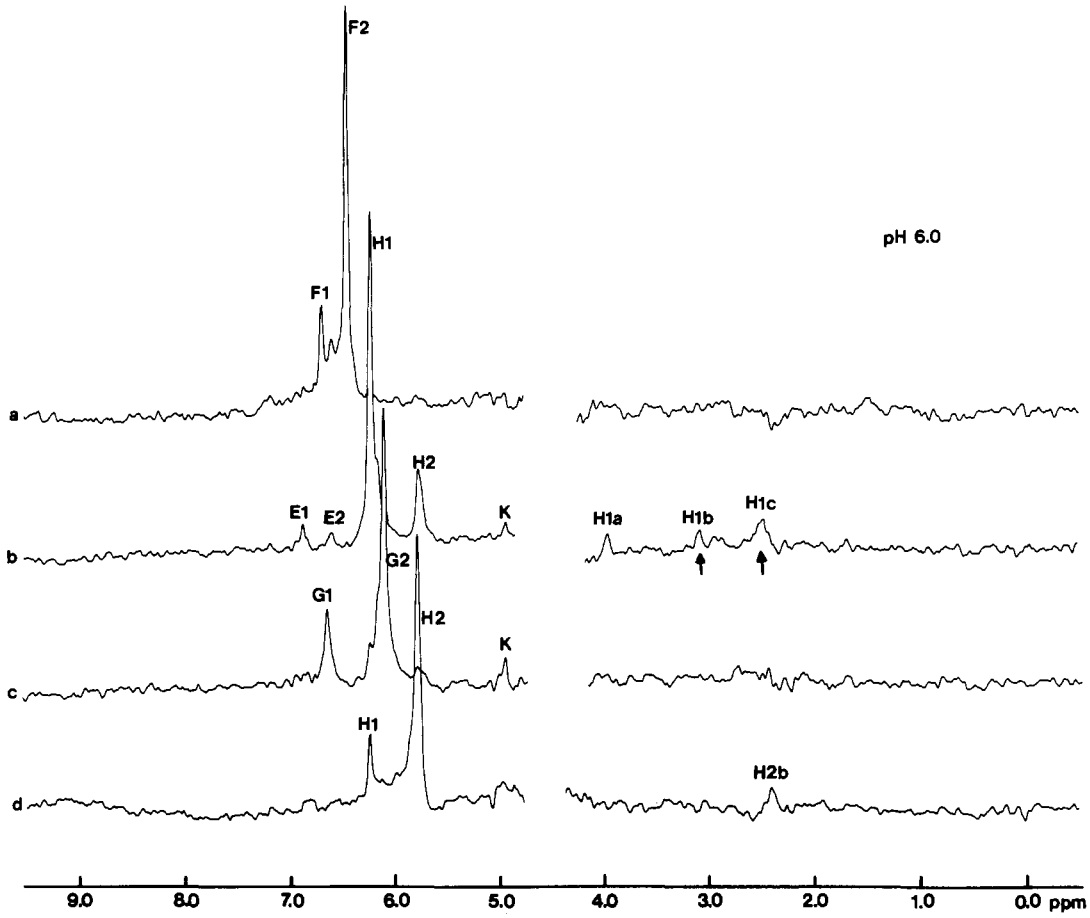

FIGURE 8: NOEs given by mEGF at pH 6.0. Four NOE difference spectra are shown, each representing the difference between an accumulation of 1500 FIDs taken with rf off-resonance and another accumulation of 1500 FIDs taken with saturating rf on-resonance. In each case, the rf saturation time was 0.4 s. Spectra are for saturation of resonance F2 (a), resonance H1 (b), resonance G2 (c), and resonance H2 (d). Conditions are the same as those in Figure 1 at pH 6.0. Resonances are labeled as described in the text.

tween these spectra (i.e., Figures 8a and 5a) cannot be observed.

Similar comparisons will now be made for the remaining tyrosine resonances irradiated. Irradiation of the Tyr-V 2,6 proton resonance (H1) (Figure 8b) at pH 6.0 produces NOEs at the Tyr-II 2,6 and 3,5 proton resonances (i.e., resonances E1 and E2, respectively), as well as the expected large NOE at its own 3,5 proton resonance (H2). This piece of structural information (i.e., a proximity relationship between Tyr-V and Tyr-II) was previously observed at pH 7.9 (Figure 5b). NOEs at the probable α-CH resonance H1a are also evident at either pH 6.0 or pH 7.9 Differences between these spectra (i.e., Figures 8b and 5b) occur with resonances H1b and H1c, probable β- or γ-CH proton resonances, and with resonance K, an α-CH proton resonance. NOEs on resonances H1b and H1c are present at either pH value but are apparently larger in magnitude at pH 6.0. An NOE on resonance K is apparent at pH 6.0, while it is lost at pH 7.9.

At pH 6.0, the Tyr-IV 3,5 proton resonance (G2) irradiation (Figure 8c) again demonstrates the expected large NOE at its own 2,6 proton resonance (G1) which is, of course, also present at pH 7.9 (Figure 5c). An obvious NOE at resonance K, an α-CH proton resonance, is present at pH 6.0 but is lost at pH 7.9 while at least two clear NOEs at resonances G2a and G2b appear only at pH 7.9 and not at pH 6.0. A proximity relationship has already been shown between Tyr-V (H2) and Tyr-IV (G2). NOE control experiments done by irradiation between resonances G2 and H2 showed an NOE on resonance H2 (i.e., the Tyr-V 3,5 proton resonance) to be partially real and partially the result of direct saturation. Approximately half of resonance H2 shown in the difference spectra in Figures 8c and 5c is the result of an NOE on this resonance. The proximity relationships (<4 Å) are maintained at either pH 6.0 or pH 7.9. An apparent NOE on resonance H1 at pH 6.0 (i.e., the Tyr-V 2,6 proton resonance) may be simply the result of direct saturation since the NOE control experiments could not differentiate between the two effects.

Proximity relationships among the Tyr-V 3,5 proton (H2), the Tyr-IV 2,6 and 3,5 protons (G1 and G2, respectively), and the α-CH proton associated with resonance K were established at pH 7.9 only be selective irradiation of resonance K (Figure 7c) with little effect seen on irradiation of resonances from the nearby residues. Differences in internal motions and numbers of protons between a tyrosine residue and a backbone α-CH proton explain variances in the observed magnitude of NOEs when one or the other proton(s) in a proximal proton pair is (are) irradiated in an NOE experiment. At pH 6.0, as noted above, NOEs on the α-CH proton resonance K are, however, observable when resonances H1 (the Tyr-V 2,6 proton resonance) and G2 (the Tyr-IV 3,5 proton resonance) are irradiated. Assuming internal motions in these residues have not changed on going from pH 7.9 to pH 6.0, a conformational change must have occurred to bring the tyrosine ring protons (i.e., the Tyr-V 2,6 and Tyr-IV 3,5 protons) into closer contact with the α-CH proton associated with resonance K.

The final resonance irradiated is resonance H2, the Tyr-V 3,5 proton resonance. In this experiment at pH 6.0 (Figure 8d), the expected NOE to its 2,6 proton resonance (H1) is observed. The only other resonance showing an NOE is the

Table II: Summary of NOE Data at pH 8.0 and 6.0

decoupled protons	peak showing NOE	pH 8.0 η (t = 0.4 s)[b]	pH 6.0 η (t = 0.4 s)[b]
Tyr-III 3,5	Tyr-III 2,6	−0.22	−0.24
Tyr-V 2,6	Tyr-V 3,5	−0.24	−0.22
	Tyr-II 2,6	−0.06	−0.08
	Tyr-II 3,5	−0.08	−0.05
	Tyr-IV 3,5	(−0.01)[a]	?
	K (α-CH)		−0.08
	H1a (α-CH or Ser β-CH_2)	−0.07	−0.07
	H1b (β- or γ-CH)	−0.05	−0.06
	H1c (β- or γ-CH)	−0.05	−0.09
Tyr-IV 3,5	Tyr-IV 2,6	−0.31	−0.28
	Tyr-V 2,6	(−0.02)[a]	
	Tyr-V 3,5	(−0.03)[a]	(−0.03)[a]
	G2a	−0.07	
	K (α-CH)		−0.21
Tyr-V 3,5	Tyr-V 2,6	−0.20	−0.23
	Tyr-II 2,6	−0.01	
	Tyr-II 3,5	−0.05	
	H2a [(H1a) α-CH or Ser β-CH_2]	−0.02	
	H2b (β- or γ-CH)		−0.08

[a] Estimates of values where partial direct saturation occurs have been corrected. [b] NOE = 1 + η; t is the mixing time.

upfield resonance H2b, a probable β- or γ-CH proton resonance. At pH 7.9, the results are dramatically different (Figure 5d). The NOE on resonance H2b is lost, while NOEs on the Tyr-II 2,6 and 3,5 proton resonances, E1 and E2, respectively, appear. Since at pH 6.0 NOEs from irradiation of the Tyr-V 2,6 proton resonance (H1) (Figure 8b) are shown on both the Tyr-II 2,6 and the Tyr-II 3,5 proton resonances (i.e., E1 and E2, respectively), the proximity relationship between Tyr-II and Tyr-V is certainly maintained at the lower pH value. The NOE data shown in Figure 5d indicate that the Tyr-II residue has somehow been reconformed with respect to the Tyr-V residue at pH 6.0. This reconformation is such that at pH 6.0 the loss of the Tyr-V 3,5 proton proximity relationship ($<\sim$4.0 Å) with the Tyr-II 2,6 and 3,5 protons has resulted in the gain of a proximity relationship with the proton(s) associated with resonance H2b.

NOE experiments in the case of the His-22 C(2) proton resonance (A1) demonstrated no observable changes on variation of the pH from 7.9 to 6.0; therefore, the data are not shown. Previous NOE data on this resonance at pH 7.4 (Figure 6b) showed no readily interpretable structural information, whereas irradiation of the His-22 C(4) proton resonance (A2) showed a proximity relationship between Tyr-3 and itself (Figure 6a). Experimental difficulties in resolving the His-22 C(4) proton resonance from others at pH values other than at around 7.4 made such comparitive experiments impossible.

Table II summarizes these NOE data and lists the magnitudes of NOEs observed at pH 8.0 and 6.0 under the same experimental conditions. The presence of an NOE under the conditions of this study usually indicates an interproton distance of approximately 3–4 Å. The absence of an NOE where one was previously observed between protons of a proximal proton pair would mean, therefore, that the interproton distance between these proximal protons has become greater than approximately 4 Å.

Discussion

Aspects of the Solution Structure. The proximity relationships between various proton pairs presented here from nuclear Overhauser measurements provide a stringent test for proposed structural models of mouse epidermal growth factor (mEGF). The most detailed model to date is that proposed by Holladay et al. (1976) on the basis of the Chou–Fasman predictive algorithm. This model, however, only provides insight into predicted aspects of protein secondary structure and is by no means infallible, especially when mostly aperiodic proteins, like mEGF, are under consideration. The Chou–Fasman model will, however, provide a starting point for our discussion.

The present data from proton NMR and nuclear Overhauser experiments lend support for the conformation of mEGF containing β-structure as evidenced by circular dichroism (CD) data and predicted by the Chou–Fasman method (Holladay et al., 1976). Merely on the basis of NOE data involving α-CH proton resonances, we identify a minimum of five or six amino acid residues as being involved in the β-sheet structure. If we accept estimates based on circular dichroism studies of 22% β-structure (Holladay et al., 1976), this corresponds to identification of approximately half the residues involved.

A Nicholson model of mEGF was constructed with β-structure at the aforementioned positions as described by Holladay et al. (1976). Much of the NOE data can be accounted for by this model. On the basis of the NOE data, three tyrosine residues (i.e., Tyr-II, -IV, and -V), one isoleucine residue (i.e., Ile-I), and the His-22 residue are conformed close to one another in the dominant mEGF solution structure. Tyr-II is proximal to Ile-I, His-22, and Tyr-V, while Tyr-V is also proximal to Tyr-IV. Tyrosines-II, -IV, and -V must also be conformed nearly linearly in order to properly explain the NOE data.

With chain reversals (β-turns) at residues 3, 6, and 10, a conformation of the NH terminus can be formed, bringing three tyrosine residues (i.e., Tyr-3, -10, and -13) into proximity (<4 Å) with one another in an almost linear array. Predicted β-turns beginning at residues 3 and 6 allow Tyr-3 and Tyr-10 to be conformed near one another, while a third β-turn at Tyr-10 places Tyr-13 within 4 Å of Tyr-10 on the opposite side of this β-turn. This conformation places Tyr-10 between Tyr-3 and Tyr-13 and allows tentative assignment of Tyr-II, -IV, and -V to Tyr-3, -13, and -10, respectively.

NOEs are also observed between the Ile-I δ-methyl proton resonance and the Tyr-3 2,6 and 3,5 proton resonances. The mere presence of these NOEs indicates interresidue distances of between 3 and 4 Å. Continuing on through the primary sequence from the NH terminus and placing a further predicted β-turn beginning at Leu-15 with a segment of β-sheet running from Val-19 to Ile-23 allows folding of the protein backbone such that Ile-23 is proximal to Tyr-3. Rotation about the isoleucine C_β–C_γ bond gives distances of closest approach from the Ile-23 δ-CH_3 to the Tyr-3 2,6 and 3,5 protons to explain the observed NOEs. Furthermore, the orientation of the phenol ring of Tyr-3 with respect to Ile-23 places the Ile-23 δ-methyl group above the plane of the ring, thus accounting for the upfield ring current shifted δ-methyl triplet resonance. A disulfide bridge between cysteine-6 and cysteine-20 pinches these two linearly separated segments together (Taylor et al., 1972), further supporting the proximity of Ile-23 and Tyr-3 suggested by the NOE data. NOE data concerning the His-22 C(4) and C(2) proton resonances (Figure 6a,b) demonstrate proximity relationships among His-22, Tyr-3, and several protons neighboring Ile-23. These data also confirm the assignment of the Ile-I δ-methyl triplet resonance to Ile-23 since only one histidine residue is present in mEGF (i.e., His-22) and it is located next to Ile-23 in the primary sequence. An NOE between His-22 and Tyr-3 places Ile-23 in the vicinity

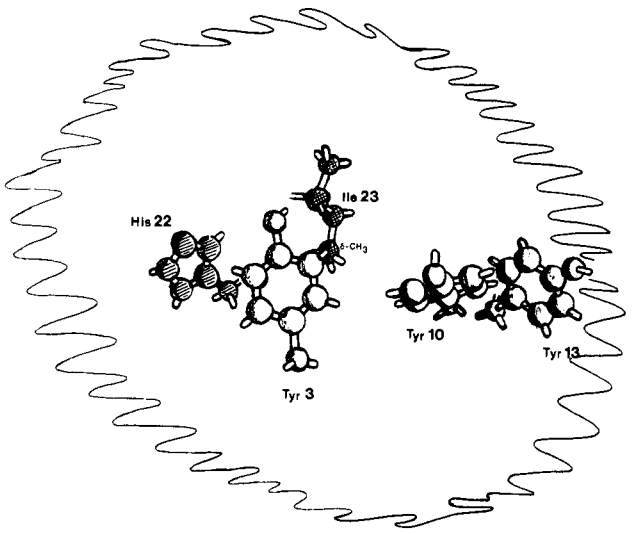

FIGURE 9: Drawing of NOE proximity relationships and a molecular outline of mEGF. Key proximity relationships in mEGF are drawn to scale for a particular molecular orientation. The only amino acid residues shown are those for which NOE data have been presented. A rough cross-sectional outline of the mEGF molecule for this particular conformation is given as a solid, squiggly line with the dimensions drawn to the same scale for the residues shown and based on model-building studies, NOE data presented here, and results presented elsewhere (Holladay et al., 1976).

of Tyr-3, and a conformation of mEGF, as previously described, can be found which brings both His-22 and Ile-23 into proximity with Tyr-3. A drawing of this above-described structural domain in mEGF involving tyrosine-3, -10, and -13, isoleucine-23, and histidine-22 is presented in Figure 9. The squiggly line in Figure 9 represents a rough cross-sectional outline of the mEGF molecule for this particular conformation.

Turning next to the NOE data from the α-CH proton resonance K (Figure 4c), it is clear that this α-CH proton is conformed in the neighborhood of Tyr-IV and -V (i.e., Tyr-13 and -10, respectively). These interproton NOEs can only be explained if both Tyr-13 and Tyr-10 exist in a tiered β-sheet conformation rather than a β-turn conformation as predicted by the Chou–Fasman algorithm (Holladay et al., 1976). In a β-turn conformation, there would be no way for one α-CH proton to be proximal to protons from two different tyrosine residues. Starting the β-sheet at Ser-9 and continuing past Tyr-13 with the β-turn starting at Tyr-10 could make a short segment of tiered β-sheet structure which would explain the observed NOEs while changing the overall predicted secondary structure only slightly.

Structural information on the remaining part of the mEGF molecule (i.e., residues 24–53) concerns NOE data involving Tyr-III, α-CH proton resonance I, and α-CH proton resonance J. The α-CH proton associated with resonance J must clearly exist in an antiparallel tiered β-sheet structure as evidenced primarily by the magnitude of the NOE from resonance J to another α-CH proton resonance, J1. The magnitude of this NOE between these two α-CH protons can only be explained in an anti-parallel β-sheet structure, where the α-CH proton from one β-sheet chain is approximately 2.6 Å apart from another α-CH proton on the opposite β-sheet chain. The regional origin of the α-CH proton associated with resonance J in mEGF remains unknown, however, since assignment either of resonance J or of any resonances showing NOEs to resonance J has not been made.

Assuming the assignments of the three previously described tyrosine residues (i.e., Tyr-3, -10, and -13) to be correct, this leaves Tyr-III to be assigned to either Tyr-29 or Tyr-37, the only two remaining tyrosine residues present in mEGF. The NOE data from the α-CH proton resonance I irradiation demonstrate it to be conformed in some type of tiered, antiparallel β-sheet structure. The magnitude of the NOE between the α-CH proton associated with resonance I and the α-CH proton resonance associated with resonance I1 falls in the range of internuclear distances between α-CH protons of opposing antiparallel β-sheet chains as was the case previously described for the α-CH proton associated with resonance J. NOEs from the α-CH proton resonance I to the Tyr-III 2,6 and 3,5 proton resonances demonstrate Tyr-III, therefore, to also exist in this tiered β-sheet structural region. Although assignment of Tyr-III to either Tyr-29 or Tyr-37 cannot, at the present time, be made, some confirmation of the predicted secondary structure as well as of the modeled tertiary structure can be gained. Both Tyr-29 and Tyr-37 are predicted by the Chou–Fasman method (Holladay et al., 1976) to be conformed in a β-sheet structure. The evidence presented here from NOE data indicates that Tyr-III, and, therefore, either Tyr-29 or Tyr-37, not only is conformed in a β-sheet structure but also exists in conjunction with another β-sheet, forming some type of tertiary, tiered antiparallel β-sheet domain, possibly like that modeled by Holladay et al. (1976).

The exact functional nature of these secondary and tertiary structural interactions is, at present, impossible to evaluate. The fact that interresidue NOEs exist, however, provides a powerful tool to examine both the solution structure of mEGF and conformational changes induced in mEGF as a function of changing environmental conditions.

pH-Induced Conformational Transition. The nuclear Overhauser data presented here also clearly demonstrate that conformational changes in the solution structure of mouse epidermal growth factor (mEGF) do occur on varying the pH from 6.0 to 8.0. The structural changes observed in a few selected cases reach the order of 1 Å. The absence of a pH-induced gross conformational change in mEGF is, however, evidenced by the facts that the great majority of NMR spectral characteristics remain nearly unchanged between pH 5.7 and 8.6 and that the proximity relationships established from NOE data among resonances of key protons examined remain, for the most part, the same between pH 6.0 and 8.0 with minor conformational modifications. Since a protein hormone's function relies strongly on maintaining an exact physical structure, this pH-induced conformational transition in mEGF, however minor, is probably functionally significant.

Two facts seem to indicate that his pH-induced conformational transition in mEGF is correlated to the breaking of the His-22 interresidue linkage ($pK_a \simeq 7.1$). First of all, lowering the pH from 8.0 to 6.0 is enough to significantly vary the observed NOEs on selective irradiation of the same resonances (i.e., resonances F2, H1, G2, and H2). With a His-22 pK_a of 7.1, only 10% of the mEGF molecular population is present as the His-22 protonated species at pH 8.1, whereas at pH 6.1, 90% of this population is present as the His-22 protonated species. The differences in these populations themselves (i.e., in the presence and absence of the His-22 interresidue linkage) are enough to explain the apparent differences in the magnitude changes of the NOE data between pH 6.0 and pH 8.0 if a conformational transition has occurred with a 50% population midpoint around pH 7.1. A conformational population of about 10% being present in an NOE experiment would, more likely than not, fall into the statistical background and not be observed. Second, and perhaps more important, is the fact that several of the resonances involved in this conformational transition between pH 6.0 and 8.0 [e.g., the Tyr-13

3,5, the Tyr-3 2,6 and 3,5 and the α-CH (K) proton resonances] reflect the His-22 pK_a of 7.1 in their chemical shift changes as a function of pH.

The full extent of these structural changes is impossible to fathom without having many more proximity relationships than presented here. It is interesting to note, however, that proximity relationships do exist among several of the proton resonances under investigation. Such proximity relationships derived from NOE data exist among Tyr-3, Tyr-10, Tyr-13, the α-CH proton associated with resonance K, Ile-23, and His-22. The Tyr-13 residue is estimated to be approximately 10 Å distant from the His-22 residue in a structural model of mEGF based on the Chou–Fasman predictive secondary structural algorithm (Holladay et al., 1976) and nuclear Overhauser (NOE) data. Several distinct interresidue distance changes occur among protons in this structural domain during the pH-induced conformational transition. Table II indicates the relative magnitude of changes in the NOEs that occur among members of this set as a function of pH.

The clearest example of a conformational change involving assigned resonances concerns changes in the orientation of Tyr-3 relative to Tyr-10. The relative orientation between these two tyrosines is significantly altered by lowering the pH from 8.0 to 6.0. At pH 6.0, the Tyr-10 3,5 proton NOEs on the Tyr-3 2,6 and 3.5 protons are lost, while the Tyr-10 2,6 proton NOEs on the Tyr-3 2,6 and 3,5 protons are modified only slightly as can be seen in Table II. Rotation of the Tyr-3 C_β–C_γ bond about the Tyr-3 α-carbon and/or the remaining part of the NH terminus containing Asn-1 and Ser-2 could explain the observed conformational change.

The only resonance examined by NOE measurements not belonging to the above-discussed N-terminal structural domain (i.e., Tyr-3, -10, and -13) is the Tyr-III 3,5 proton resonance. Tyr-III can be assigned to either Tyr-29 or Tyr-37 in mEGF. NOE data have demonstrated that Tyr-III exists in some form of tiered β-sheet structure which, on the basis of model-building studies, is present on the opposite side of the mEGF molecule from the above-discussed structural domain (i.e., Tyr-3, -10, and -13). As evidenced by invariances in the NOE difference spectra concerning the Tyr-III 3,5 proton resonance (i.e., F2) shown in Figures 8a and 5a for pH 6.0 and 7.9, respectively, and the absence of significant chemical shift changes in resonances associated with residues other than those in this N-terminal domain (i.e., Tyr-3, -10, and -13), this pH-induced conformational transition in mEGF may well be localized around the N-terminal structural domain. It should also be noted that the aforementioned minor spectral resonances are associated with protons of amino acid residues (i.e., Tyr-10 and -13 and His-22) which belong to this same N-terminal domain.

The biological significance of this conformational transition in mEGF on breaking the His-22 interresidue linkage remains to be explained. Several lines of evidence indicate that mouse epidermal growth factor (mEGF) exists in vivo as a high molecular weight tetrameric complex composed of two molecules of mEGF and two molecules of a binding protein (29 300 daltons) (Taylor et al., 1970, 1974a). The mEGF binding protein exhibits an arginine esterase activity which could be responsible for some type of posttranslational modification of a higher molecular weight precursor form of mEGF since mEGF possesses a C-terminal arginine residue. Both the binding of mEGF to its binding protein and the arginine esterase activity of the binding protein itself are pH sensitive (Taylor et al., 1974a,b). The arginine esterase activity is maximal between pH 7.8 and 8.5 and falls off to approximately 10% of the original activity at pH 5.5, with 50% activity being maintained around pH 7.0. It seems possible, therefore, that at least part of the biological significance of the observed conformational transition in mEGF is somehow correlated with the pH-induced effects on the mEGF–binding protein complex. The pH dependence of mEGF binding to its cellular transmembrane receptor would make an interesting study.

Acknowledgments

Professor Stanley Cohen, Vanderbilt University, is gratefully acknowledged for provision of mouse epidermal growth factor, helpful discussions, and reading of the manuscript. Many special thanks to Prof. J. H. Prestegard for his support and guidance and for his critical review of the manuscript.

Registry No. mEGF, 62229-50-9.

References

Billeter, M., Braun, W., & Wüthrich, K. (1982) *J. Mol. Biol. 152*, 321–345.

Buhrow, S. A., Cohen, S., & Staros, J. V. (1982) *J. Biol. Chem. 257*, 4019–4022.

Buhrow, S. A., Cohen, S., Garbers, D. L., & Staros, J. V. (1983) *J. Biol. Chem. 258*, 7824–7827.

Bundi, A., & Wüthrich, K. (1979) *Biopolymers 18*, 279–285.

Carpenter, G., & Cohen, S. (1976) *J. Cell Biol. 71*, 159–171.

Carpenter, G., & Cohen, S. (1979) *Biochem. Actions Horm. 5*, 121–156.

Carpenter, G., Lemback, K. J., Morrison, M. M., & Cohen, S. (1975) *J. Biol. Chem. 250*, 4297–4304.

Chapman, G. E., Abercrombie, B. D., Cary, P. D., & Bradbury, E. M. (1978) *J. Magn. Reson. 31*, 459–468.

Chou, P. Y., & Fasman, G. D. (1974a) *Biochemistry 13*, 211–221.

Chou, P. Y., & Fasman, G. D. (1974b) *Biochemistry 13*, 222–245.

Chou, P. Y., & Fasman, G. D. (1978a) *Annu. Rev. Biochem. 47*, 251–276.

Chou, P. Y., & Fasman, G. D. (1978b) *Adv. Enzymol. Relat. Areas Mol. Biol. 48*, 45–148.

Cohen, S. (1962) *J. Biol. Chem. 237*, 1555–1562.

Cohen, S. (1965) *Dev. Biol. 12*, 394–407.

Cohen, S., & Elliott, G. A. (1963) *J. Invest. Dermatol. 40*, 1–5.

Cohen, S., & Savage, C. R., Jr. (1974) *Recent Prog. Horm. Res. 30*, 551–572.

Cohen, S., & Taylor, J. M. (1974) in *Thirtieth Symposium of the Society of Developmental Biology* (Hay, E. D., King, T. J., & Papaconstantinous, J., Eds.) pp 25–42, Academic Press, New York.

Cohen, S., Carpenter, G., & Lembach, K. J. (1975) *Adv. Metab. Disord. 8*, 265–284.

Dobson, C. M., Hoch, H. C., Olejniczak, E. T., & Poulsen, F. M. (1980) *Biophys. J. 32*, 325–636.

Gordon, S., & Wüthrich, K. (1978) *J. Am. Chem. Soc. 100*, 7094–7098.

Holladay, L. A., Savage, C. R., Cohen, S., & Puett, D. (1976) *Biochemistry 15*, 2624–2633.

Hollenberg, M. D., & Cuatrecasas, P. (1973) *Proc. Natl. Acad. Sci. U.S.A. 70*, 2964–2968.

Kalinichenko, P. (1976) *Stud. Biophys. 58*, 235–240.

Krishna, N. R., Agresti, D. G., Glickson, J. D., & Walter, R. (1978) *Biophys. J. 24*, 791–802.

Mayo, K. H., Tyrell, P. M., & Prestegard, J. H. (1983) *Biochemistry 22*, 4485–4493.

McKanna, J. A., Haigler, H. T., & Cohen, S. (1979) *Proc. Natl. Acad. Sci. U.S.A. 76*, 5689–5693.

Noggle, J. H., & Shirmer, R. E. (1971) *The Nuclear Overhauser Effect*, Academic Press, New York.
Oldfield, E., Norton, R. S., & Allerhand, A. (1975) *J. Biol. Chem. 250*, 6368–6375.
Poulsen, F. M., Hoch, J. C., & Dobson, C. M. (1980) *Biochemistry 19*, 2597–2601.
Savage, C. R., Jr., & Cohen, S. (1972) *J. Biol. Chem. 247*, 7609–7611.
Savage, C. R., Jr., & Cohen, S. (1973) *Exp. Eye Res. 15*, 361–366.
Savage, C. R., Jr., Hash, J. H., & Cohen, S. (1973) *J. Biol. Chem. 248*, 7669–7672.
Sykes, B. D., Weingarten, H. I., & Schlesinger, M. J. (1974) *Proc. Natl. Acad. Sci. U.S.A. 71*, 469–474.
Taylor, J. M., Cohen, S., & Mitchell, W. M. (1970) *Proc. Natl. Acad. Sci. U.S.A. 67*, 164–171.
Taylor, J. M., Mitchell, W. M., & Cohen, S. (1972) *J. Biol. Chem. 247*, 5928–5934.
Taylor, J. M., Mitchell, W. M., & Cohen, S. (1974a) *J. Biol. Chem. 249*, 2188–2194.
Taylor, J. M., Mitchell, W. M., & Cohen, S. (1974b) *J. Biol. Chem. 249*, 3198–3203.
Turkington, R. W. (1969) *Exp. Cell Res. 57*, 79–85.
Wagner, g., & Wüthrich, K. (1979) *J. Magn. Reson. 33*, 675–687.
Wüthrich, K., Wider, G., Wagner, G., & Braun, W. (1982) *J. Mol. Biol. 152*, 311–320.

(23*S*)-1,23,25-Trihydroxyvitamin D_3: Its Biologic Activity and Role in 1α,25-Dihydroxyvitamin D_3 26,23-Lactone Biosynthesis†

Ronald L. Horst,* Peter M. Wovkulich, Enrico G. Baggiolini, Milan R. Uskokovič, George W. Engstrom, and Joseph L. Napoli

ABSTRACT: (23*S*)-1,23,25-Trihydroxyvitamin D_3 was isolated from bovine kidney homogenates incubated with 1,25-dihydroxyvitamin D_3 by sequential chromatography through one Sephadex LH-20 column and three high-performance liquid chromatography systems. Ultraviolet absorption spectroscopy and mass spectrometry confirmed the structural assignment. One high-performance liquid chromatography system separated the *R* and *S* epimers of 1,23,25-trihydroxyvitamin D_3 and indicated that the natural product had the *S* configuration. Plasma pharmacokinetic studies in rats showed that (23*S*)-1,23,25-trihydroxy[^{3}H]vitamin D_3 was rapidly cleared from plasma ($t_{1/2}$ = 60 min). 1α,25-Dihydroxy[^{3}H]vitamin D_3 26,23-lactone appeared concurrently with the disappearance of (23*S*)-1,23,25-trihydroxy[^{3}H]vitamin D_3. Experiments with radioinert compounds showed that 1,25-dihydroxyvitamin D_3 and (23*S*)-1,23,25-trihydroxyvitamin D_3 were efficient precursors to 1,25-dihydroxyvitamin D_3 26,23-lactone both in intact and in nephrectomized rats. (25*S*)-1,25,26-Trihydroxyvitamin D_3, however, was ineffective at raising plasma 1,25-dihydroxyvitamin D_3 26,23-lactone concentrations. These results confirm the presence of extrarenal 1,25-dihydroxyvitamin D_3 23(*S*)-hydroxylase(s) and demonstrate that C-23 hydroxylation of 1,25-dihydroxyvitamin D_3 precedes C-26 hydroxylation in the formation of 1,25-dihydroxyvitamin D_3 26,23-lactone. (23*S*)-1,23,25-Trihydroxyvitamin D_3 had no intestinal calcium absorptive or bone calcium resorptive activity when dosed to vitamin D deficient rats at levels up to 500 ng. C-23 oxidation, therefore, appears to be a physiologic pathway of 1,25-$(OH)_2D_3$ metabolism and a major pathway for the deactivation of pharmacologic levels of 1,25-dihydroxyvitamin D_3.

During normal nutrition or hypervitaminosis D, the most abundant vitamin D metabolite in the plasma is 25-hydroxyvitamin D (25-OHD).[1] Oxidation of 25-OHD at C-1, C-24, and C-26 results in the formation of 1,25-$(OH)_2D_3$, (24*R*)-24,25-$(OH)_2D_3$, and (25*S*)-25,26-$(OH)_2D_3$. These metabolites circulate in plasma under physiological conditions (Horst et al., 1981a; Napoli et al., 1981; Partridge et al., 1981a). A hormonal form of vitamin D_3, 1,25-$(OH)_2D_3$, is similarly metabolized at C-24 and C-26 to form (24*R*)-1,24,25-$(OH)_3D_3$ and (25*S*)-1,25,26-$(OH)_3D_3$ (Holick et al., 1973; Partridge et al., 1981b; Reinhardt et al., 1981, 1982). Under normal vitamin D nutrition, nephrectomy prevents the formation of 24-hydroxylated vitamin D_3 metabolites and lactone. However, 24-oxidized compounds and lactone reappear in nephrectomized animals given an excess of vitamin D_3 (Horst et al., 1981a; Horst & Littledike, 1980).

The first evidence for vitamin D C-23 oxidative pathways surfaced with the identification of the lactones of 25-OHD_3 and 1,25-$(OH)_2D_3$ (Horst, 1979; Wichmann et al., 1979; Ishizuka et al., 1981). Subsequently, the compounds (23*S*)-23,25-$(OH)_2D_3$ and (23*R*)-23,25-$(OH)_2D_3$ were chemically

† From the Physiopathological Research Laboratory, National Animal Disease Center, Agricultural Research Service, U.S. Department of Agriculture, Ames, Iowa 50010 (R.L.H. and G.W.E.), the Department of Natural Products Chemistry, Hoffmann-La Roche, Inc., Nutley, New Jersey 07110 (P.M.W., E.G.B., and M.R.U.), and the Department of Biochemistry, The University of Texas Health Science Center, Dallas, Texas 75235 (J.L.N.). *Received November 10, 1983.*

[1] Abbreviations: 25-OHD, 25-hydroxyvitamin D; 1,25-$(OH)_2D_3$, 1,25-dihydroxyvitamin D_3; 24,25-$(OH)_2D_3$, 24,25-dihydroxyvitamin D_3; 25,26-$(OH)_2D_3$, 25,26-dihydroxyvitamin D_3; 1,24,25-$(OH)_3D_3$, 1,24,25-trihydroxyvitamin D_3; 1,25,26-$(OH)_3D_3$, 1,25,26-trihydroxyvitamin D_3; 25-OHD_3, 25-hydroxyvitamin D_3; 23,25-$(OH)_2D_3$, 23,25-dihydroxyvitamin D_3; lactone, 25-hydroxyvitamin D_3 26,23-lactone; 1,23,25-$(OH)_3D_3$, 1,23,25-trihydroxyvitamin D_3; HPLC, high-performance liquid chromatography; GC/MS, gas chromatography/mass spectrometry; HEPES, 4-(2-hydroxyethyl)-1-piperazineethanesulfonic acid; EI, electron impact.